Biomatter 5:1, e1005527; May 2015; Published with license by Taylor & Francis Group, LLC

Cell infiltration into a 3D electrospun fiber and hydrogel hybrid scaffold implanted in the brain

Christopher J Rivet[1,*], Kun Zhou[2], Ryan J Gilbert[1], David I Finkelstein[3], and John S Forsythe[2]

[1]Center for Biotechnology and Interdisciplinary Studies; Department of Biomedical Engineering; Rensselaer Polytechnic Institute; Troy, NY USA; [2]Department of Materials Science and Engineering, Monash Institute of Medical Engineering, Faculty of Engineering; Monash University; Clayton, Australia; [3]Florey Institute of Neuroscience and Mental Health; University of Melbourne; Melbourne, Australia

Tissue engineering scaffolds are often designed without appropriate consideration for the translational potential of the material. Solid scaffolds implanted into central nervous system (CNS) tissue to promote regeneration may require tissue resection to accommodate implantation. Or alternatively, the solid scaffold may be cut or shaped to better fit an irregular injury geometry, but some features of the augmented scaffold may fail to integreate with surrounding tissue reducing regeneration potential. To create a biomaterial able to completely fill the irregular geometry of CNS injury and yet still provide sufficient cell migratory cues, an injectable, hybrid scaffold was created to present the physical architecture of electrospun fibers in an agarose/methylcellulose hydrogel. When injected into the rat striatum, infiltrating macrophages/microglia and resident astrocytes are able to locate the fibers and utilize their cues for migration into the hybrid matrix. Thus, hydrogels containing electrospun fibers may be an appropriate platform to encourage regeneration of the injured brain.

Keywords: brain, electrospun fibers, hydrogel, neuroengineering

*Correspondence to: Christopher J Rivet; Email: chrisjrivet@gmail.com; John S Forsythe; Email: John.Forsythe@Monash.edu

Submitted: 05/12/2014

Revised: 08/02/2014

Accepted: 01/05/2015

http://dx.doi.org/10.1080/21592535.2015.1005527

Introduction

Tissue loss due to traumatic brain injury or neurodegenerative diseases is particularly difficult to reconcile given the central nervous system's (CNS) inherently limited capacity for self-renewal due the presence of the glial scar,[1,2] however, even within this environment regeneration is possible.[3] Biomaterial scaffolds are shown to assist in tissue regeneration by providing physical and chemical cues to direct cellular infiltration into the lesion, or implant site, in the brain[4,5] and spinal cord.[6,7] Although the results to date are promising, there is a substantial deficit in the translational quality of the scaffolds in that solid scaffolds (e.g. electrospun fibers) require tissue resection for placement and soft scaffolds (e.g., hydrogels) lack physical structures to facilitate cellular migration - outside of the passiveness attributed to porosity. However, both electrospun fibers and hydrogels present unique attributes; electrospun fibers present cellular-scale topographical cues and hydrogels are injectable. Thus, a hybrid scaffold that synergistically combines electrospun fibers within a hydrogel was created to overcome the limitations of both approaches.

Electrospun fibers are in widespread use for neuroengineering applications; *in vitro*, the physical features direct neuronal differentiation of stem cells[8,9] and enhance neurite outgrowth.[10] When *in vivo*, the fibers interact with both neurons and astrocytes to the extent of fostering tissue regeneration in the spinal cord[11] and brain.[12] The electrospinning process presents a number of fabrication parameters that permit production of substrates with specific qualities (i.e. fiber diameter, alignment, chemistry, etc.).[13] However, presenting these qualities to the *in vivo* environment is difficult given their thin, sheet-like configuration. Rolling the material into a tubular structure is the most common approach,[11,12] however tubular structures require tubular injury geometries for implantation and may require a separate cell transplantation process to place cells within the scaffold.[14]

Similarly, hydrogels are reported in many *in vitro* trials for stem cell differentiation, where the mechanical and chemical properties are manipulated to promote neuronal lineages by replicating the CNS tissue modulus.[15,16] Hydrogels possess features making them desirable for *in vivo* CNS applications; a liquid is delivered via syringe and needle, minimally disrupting local tissue and conforming to the irregular lesion geometry. However, a major drawback of some hydrogels is that the hydrogel matrix does not present cellular-scale architecture to permit strong cellular adhesion and induce subsequent cellular infiltration for the rapid repair of tissues.[17]

There are a number of studies that attempt to increase electrospun fiber and hydrogel clinical relevance by altering the physical properties given the aforementioned limitations of both systems. For example, electrospun fibers display a high aspect ratio (e.g. diameter to length), which creates a dense, impenetrable mat. Increasing the inter-fiber spacing, or porosity, is accomplished by addition of sacrificial pore forming agents,[18-21] but even these electrospun fibers are not injectable nor can they completely fill a void created when CNS tissue is damaged. Electrospun fibers can be deposited into 3D macrostructures[22] and are also added to hydrogels to present physical features in a synergistic manner,[23-26] however, to date these attempts are largely unsuccessful and do not present a truly translational approach.

To this end, an innovative approach to place individual fibers within a hydrogel is presented. To encourage cell adhesion to the injected fibers,[27] fibronectin was electrospun with the polymer poly-L-lactide (PLLA) to create fibronectin/PLLA composite fibers. PLLA electrospun fibers with and without fibronectin inclusion were dispersed in an agarose/methylcellulose hydrogel at 2 distinct densities (low and high). The agarose/methylcellulose combination was used given its injectability, physiologically relevant thermogelation properties, and biocompatibility.[28] Furthermore, the cellulose-based materials will not significantly degrade over the course of the study, allowing for isolation of electrospun fiber topography-induced infiltration from hydrogel degradation-induced infiltration. The hybrid scaffold was implanted within the rat striatum to provide proof of concept that the scaffold was injectable and to discern if fibronectin inclusion enhanced cellular recognition of the injected fibers. We present a new biomaterial strategy to encourage cellular infiltration into the lesion site following brain injury.

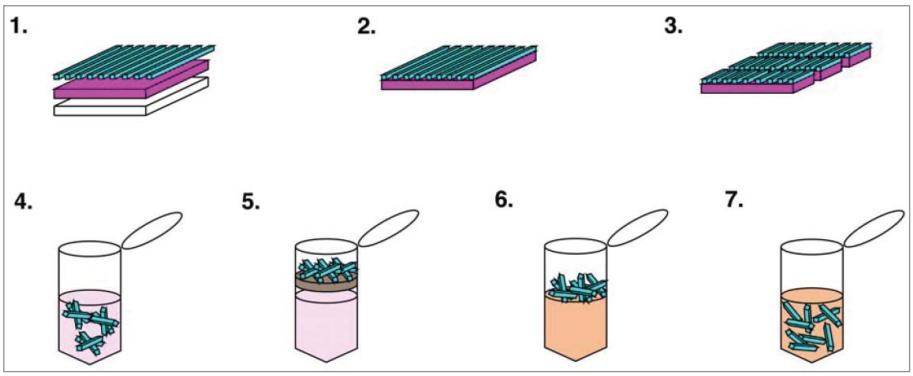

Figure 1. Schematic of isolation and dispersion of electrospun fibers within a hydrogel matrix. (1) Aligned electrospun fibers were collected on a thin film of polyvinylalcohol (PVA), which was evaporation cast onto a 15 mm square glass slide. (2) The thin film with fibers attached was removed from the glass substrate. (3) The thin film with fibers attached was cut into short segments (1 mm) perpendicular to fiber alignment. (4) Strips of thin film and fiber were placed into a microcentrifuge tube containing ddH_2O to selectively dissolve the PVA. (5) The solution was transferred to a 0.45 μm microcentrifuge filter to separate the fibers segments from the PVA solution. (6) The fiber segments were transferred to a microcentrifuge tube containing hydrogel. (7) The fibers were dispersed within the hydrogel by repeatedly passing the mixture through a syringe.

Results and Discussion

Electrospun PLLA fibers and PLLA + fibronectin fibers, **Figure S1**, were first characterized in their as-produced, 2D format to determine the effects of adding fibronectin to the PLLA electrospinning solution and subsequent fiber appearance and geometry. Fibronectin increases the electrospinning solution conductivity, thus PLLA + fibronectin fiber diameter was 0.84 ± 0.20 μm and PLLA was 1.26 ± 0.18 μm. Fiber alignment variance and fiber density were not significantly different based on the presence/absence of fibronectin (due to the alteration of fiber collection time). Thus, there were no differences in fiber density between the plain fibers and the fibronectin fibers groups; therefore differences in cellular infiltration could not be attributed to differences in fiber density.

The 2D fiber images also provide a reference point for the visual transformation that occurs when the fibers undergo processing for dispersion throughout the hydrogel matrix (e.g., the 2D to 3D transition), **Figure 1**. Fluorescent electrospun PLLA fibers were created and dispersed throughout the hydrogel matrix to aid in visualization, **Figure 2**. Hybrid scaffolds were created with low fiber density, **Figure 2A**, and high fiber density, **Figure 2B**. This new process of placing electrospun fibers within a hydrogel provides great control over fiber density, fiber type, and hydrogel type, with many combinations possible. Hsieh et al.[25] also presented a technique for dispersing electrospun fibers within a hydrogel, however, the approach presented here appears to greatly increase the density of fibers within the hydrogel.

Four experimental scaffold compositions were created, all of which were dispersed in the agarose/methylcellulose hydrogel: PLLA fibers – low density, PLLA fibers – high density, PLLA + fibronectin fibers – low density, and PLLA + fibronectin fibers – high density. A blank agarose/methylcellulose hydrogel and a sham, saline injection served as controls. Scaffolds were implanted bilaterally into the rat striatum with a 5-minute delay added between implantation and needle retraction to accommodate initial

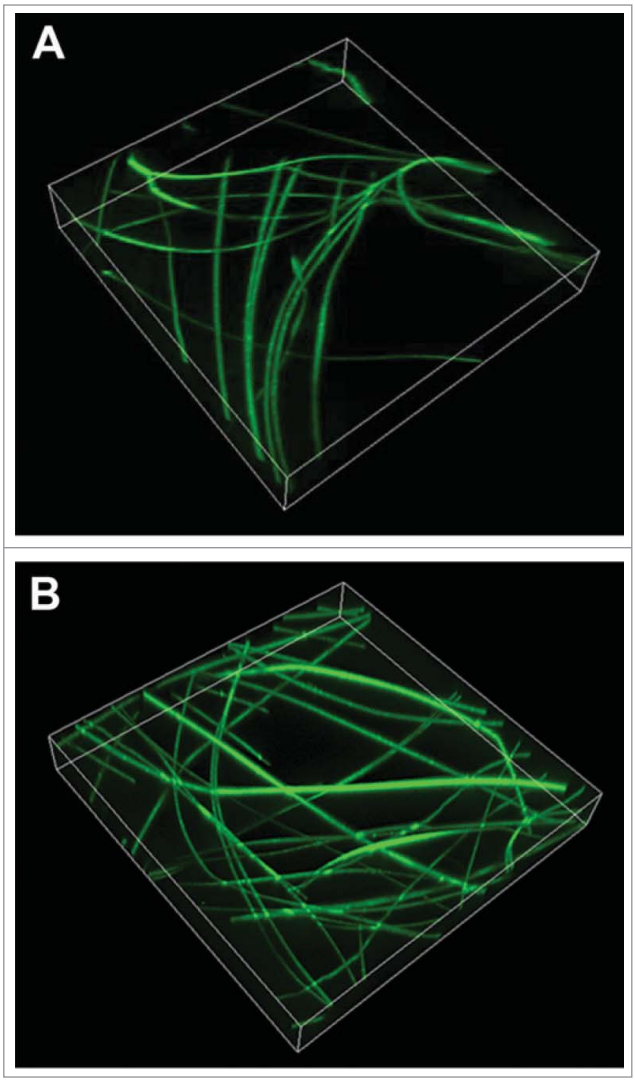

Figure 2. 3D rendering of fluorescent electrospun fibers dispersed in an agarose/methylcellulose hydrogel at 2 densities. Electrospun fibers doped with rhodamine-123 were electrospun and incorporated into the hydrogel at (**A**) low and (**B**) high densities. Low density samples combine 5 coverslips of fibers per 500 μL of hydrogel whereas high density samples combine 10. Images were captured using a 20X objective lens through 50 μm in the Z-direction. The 3D rendered images were created using the 4D function in MetaMorph.

gelation, ensuring that the scaffold would not leak out along the injection tract. Implant geometry for all sample types was retained over the 60-day period as seen in **Figure 3**. The sham control (e.g., saline injection, data not shown) did not retain the injection tract geometry and was only distinguishable from the surrounding tissue by a slight increase in the number of glial fibrillary acid protein (GFAP+) astrocytes.

Retention of the implant shape, and lack of lesion volume reduction, in all scaffold samples could be due to 2 distinct reasons: the implanted material inhibited tissue regeneration and/or the tissue itself cannot regenerate. The former was more likely to occur than the latter. Cellulose-based hydrogels have a limited capacity for degradation; physical dissociation was the only means for implant size reduction. A study by Stokols et al.[29] reporting a similar cellulose-based scaffold implanted within the CNS displayed resilience to degradation for at least one month. Tissue regeneration within the CNS was possible, as reported by Villapol et al.[30] where significant reduction in lesion volume size over a 60-day period in a model of traumatic brain injury occurred, however, this model was located in the cortex and in the absence of an inhibitory hydrogel. Thus, the lack of lesion volume reduction for the duration of this study was anticipated due to the resilience of the cellulose-based hydrogel, even in an environment capable of reducing lesion size.

The tissue-implant interface, **Figure 4** (from demarcated regions in **Fig. 3**), was quantified for astrocyte accumulation as a function of implant composition at 3 time points: 7, 21, and 60 d post implantation; however, statistical significance was not found, **Figure S2**. Using a resilient material provides clear evidence of electrospun fiber-induced infiltration at the interface, whereas if a degradable hydrogel (e.g., collagen, fibrin, etc.) were used, it would be difficult to distinguish the degradation-induced infiltration from the topography-induced infiltration. In **Figure 4C and E** extensive astrocyte and macrophage/microglia infiltration was displayed in comparison to **Figure 4A, B, and D**. This corresponds to the PLLA + fibronectin fiber samples promoting cellular infiltration. Co-localization of infiltrating cells with electrospun fibers was further validated in **Figure S3.**

Migrating astrocytes were previously shown to be indicative of increased tissue regeneration in a spinal cord injury model.[11] The astrocytes in **Figure 4E** display a markedly different morphology to those in **Figure 4B**. Astrocytes in **Figure 4E** were protruding into the lesion whereas in **Figure 4B** astrocytes were perpendicular to the lesion boundary, creating a physical barrier similar to the glial scar. The astrocyte morphology in **Figure 4E** may be indicative of increased regenerative potential, however, when an antibody for neurofilament was applied, neurite projections into the scaffolds were not found, **Figure 5**. The aforementioned differences in astrocyte morphology were more clearly visualized in **Figure 5B and E**. When considering the changes in astrocyte morphology in response to electrospun fiber topography and their reported effects,[11,27] there may be an increased potential for regeneration even though significant neurite infiltration was not found. The astrocytes were in contact with the

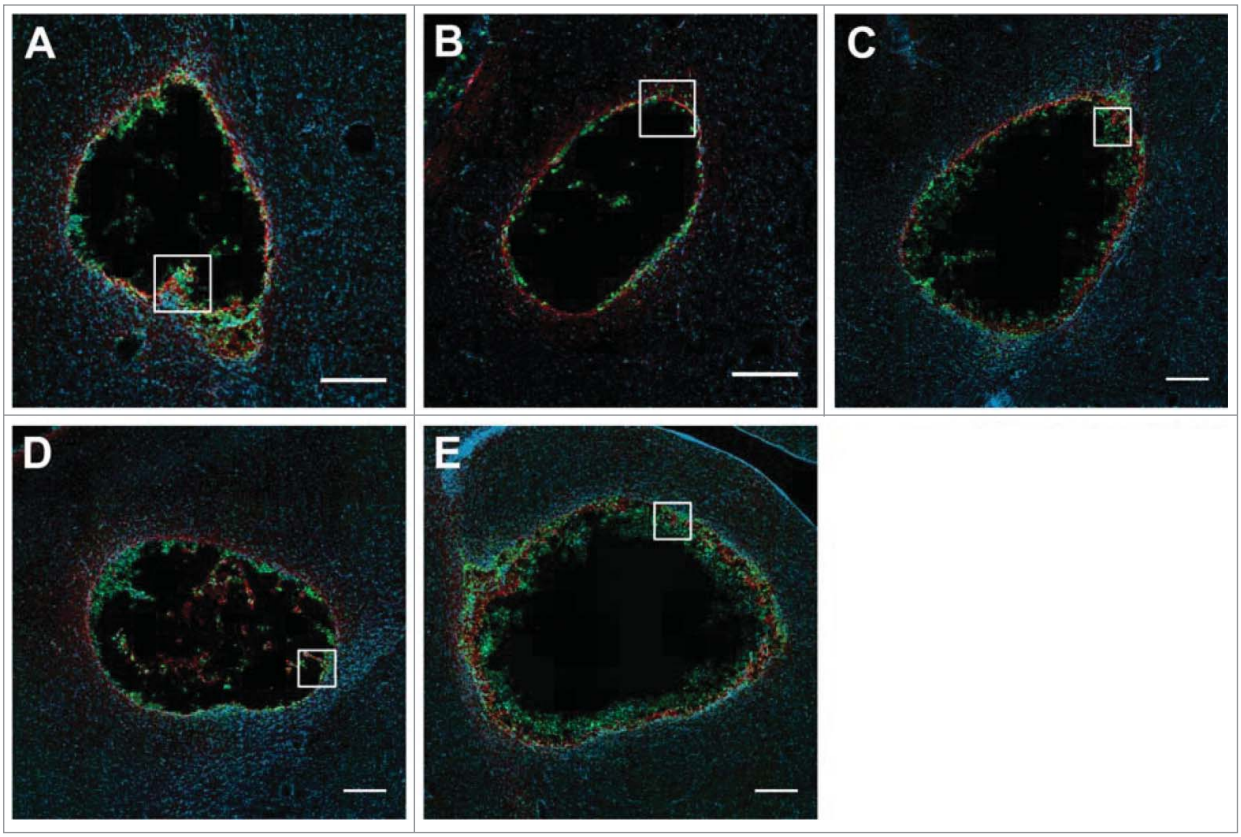

Figure 3. Implant geometry 60 d post implantation. The tissue was sectioned transverse to the injection tract, displaying the cross sectional area of each implant, and stained for astrocytes (GFAP, red), macrophages/microglia (ED1, green), and nuclei (DAPI, blue). The samples were as follows: (**A**) Blank hydrogel, (**B**) PLLA fibers – low density, (**C**) PLLA + fibronectin fibers – low density, (**D**) PLLA fibers – high density, and (**E**) PLLA + fibronectin – high density. The cross sectional area for each implant was not significantly altered as a function of time or scaffold composition. Demarcated areas indicate the regions captured at high magnification for **Figure 4**. Images were captured with a 10X objective lens using the slide scan function in MetaMorph. Z-stack ranges were optimized for each fluorescence channel and captured independently. Scale bars represent 250 μm.

electrospun fibers; if they were able to infiltrate further into the matrix, it may be possible that neurites would follow, such as in the case of Nisbet et al.[12] This study provided validation that electrospun fiber topography can be implanted in an unobtrusive manner and can be recognized and utilized by interfacing cells.

There are numerous investigations where novel materials with sophisticated chemistries are developed for tissue engineering strategies, however, few place due importance on the translational quality of the material. In this study, the primary objective was to develop a tissue engineering scaffold that minimizes implantation-associated trauma and maximizes cellular infiltration. Thus, by combining the injectable qualities of hydrogels with the physical guidance cues of electrospun fibers such a material was created. The fabrication process is easily altered to accommodate any hydrogel or electrospun fiber of interest, enabling scaffold creation for all tissue engineering applications.

Methods and Materials

Electrospun fiber fabrication

A polyvinylalcohol (PVA) thin film to serve as an electrospun fiber collection substrate was prepared by evaporation casting a 1:1 volumetric ratio of Partall® PVA solution (Rexco) and ethanol onto 15 × 15 mm glass coverslips and air-dried overnight. A method for incorporating protein into the polymeric matrix was adopted from Koh et al.[31] In brief, electrospinning solution consisted of 1,1,1,3,3,3-hexafluoro-2-propanol (HFIP, Sigma-Aldrich), dimethylsulfoxide (DMSO, Sigma-Aldrich), and 12% (wt./wt.) poly-L-lactide (PLLA, Natureworks™; grade 6201D, Cargill Dow LLC). Fibronectin (Sigma-Aldrich) was dissolved into the DMSO portion at 0.5 mg/mL and added to HFIP at a volumetric ratio of 7.33:1. Electrospinning parameters, using a previously described apparatus,[10] were as follows: 9 kV, 1000RPM rotational velocity, 6 cm needle-target separation, 2.03 mL/hr flow rate, 22 gauge insulated needle, 3 minutes collection duration for fibers with fibronectin (5 minutes without), and 18–22% relative humidity. One fiber sample from 3 independently fabricated batches was used for analysis of fiber diameter ($n = 30$), alignment variation ($n = 3$), and density ($n = 9$) in accordance with previously outlined procedures.[10] A Tukey-Kramer HSD test was performed on JMP (SAS) software to determine statistical significance ($P < 0.05$).

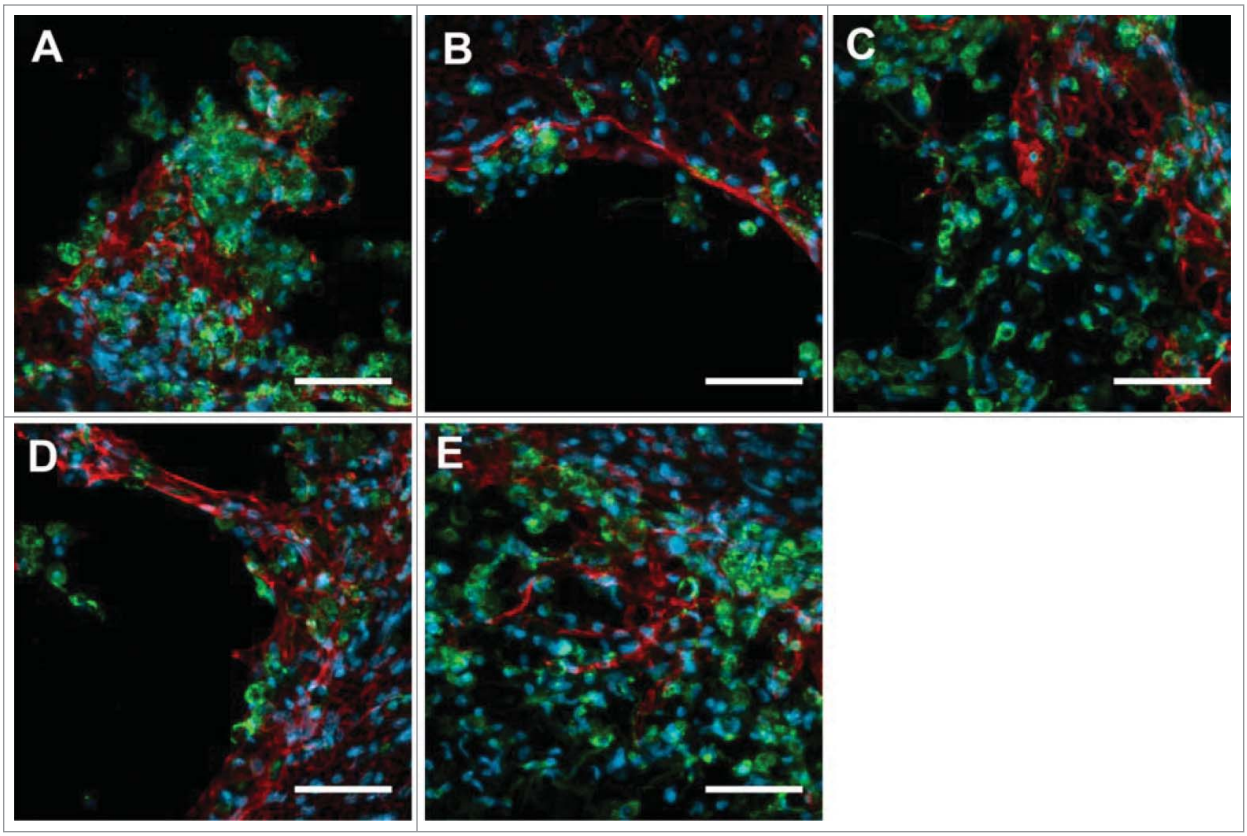

Figure 4. Astrocyte and macrophage/microglia interactions with hybrid scaffolds implanted into the striatum 60 d post implantation. High magnification images (demarcated areas of corresponding images in **Fig. 3**) of astrocytes (GFAP, red) and macrophages/microglia (ED1, green) at the tissue-scaffold interface display cellular infiltration into the hybrid scaffold and utilization of the electrospun fiber network. Nuclei were labeled with DAPI (blue). The samples were as follows: (**A**) Blank hydrogel, (**B**) PLLA fibers – low density, (**C**) PLLA + fibronectin fibers – low density, (**D**) PLLA fibers – high density, and (**E**) PLLA + fibronectin – high density. The fibronectin fiber samples, (**C and E**), display a greater extent of cellular infiltration into the hybrid matrix as well as a more loosely defined glial boundary as compared to that displayed in B. Images were captured with a 40X objective lens. Z-stack ranges were optimized for each fluorescence channel and captured independently. Scale bar represents 50 μm.

Fluorescent electrospun fibers were created from a 1:1 solution of chloroform and dichloromethane with 8% (wt./wt.) PLLA. A 2.5 mg/mL solution of rhodamine-123 (Sigma-Aldrich) in DMSO was prepared and added to the electrospinning solution at a volumetric ratio of 1:1000 one hour prior to electrospinning. Electrospinning parameters were the same as outlined above, but with the following adjustments: collection time is increased to 10 minutes and relative humidity was increased to 40%.

Hybrid electrospun/hydrogel fabrication

A hydrogel composed of 1.5% SeaPrep (Lonza) agarose and 7.0% Methocel (Dow Chemical) methylcellulose was created in a manner similar to that of Martin et al.[28] Electrospun fibers as produced in the preceding sections were dispersed into the hydrogel matrix by first removing the PVA film with fibers from the coverglass substrate, cutting the samples perpendicular to fiber alignment into 1.0 mm wide strips, and dissolving the PVA substrate overnight in water. The solution was passed through 22 gauge and then 26 gauge needles by a 1mL syringe to disrupt the fiber strips. A 0.45 μm microcentrifuge filter was used to isolate the fibers from the PVA solution. The fibers were washed with deionized water to remove the residual PVA and then sterilized by 80% ethanol for 15 minutes before subsequent centrifugation. The dry, sterilized fibers were then removed from the filter membrane, placed onto 500 μL of hydrogel in a 2.0 mL microcentrifuge tube (10 coverslips of fibers for high density and 5 for low density), drawn into a 1 mL slip-tip syringe with the needle removed, and forcefully dispensed back into the microcentrifuge tube multiple times to disperse the fibers throughout the gel. Each sample was then passed through a 26 g needle to ensure full dispersion. All samples were kept on ice until the point of application.

Animals and implantation procedure

All procedures were approved by the institutional ethics committee (Florey Neuroscience Institute Animal Ethics Committee) and conform to national and international standards of care for experimental animals. Scaffolds were bilaterally implanted into the striatum of 36 male Wistar rats (72 samples in total). Implants consisted of: (1) agarose/methylcellulose hydrogel (Blank), (2) PLLA fibers - low density in hydrogel, (3) PLLA fibers - high density in hydrogel, (4) PLLA + fibronectin

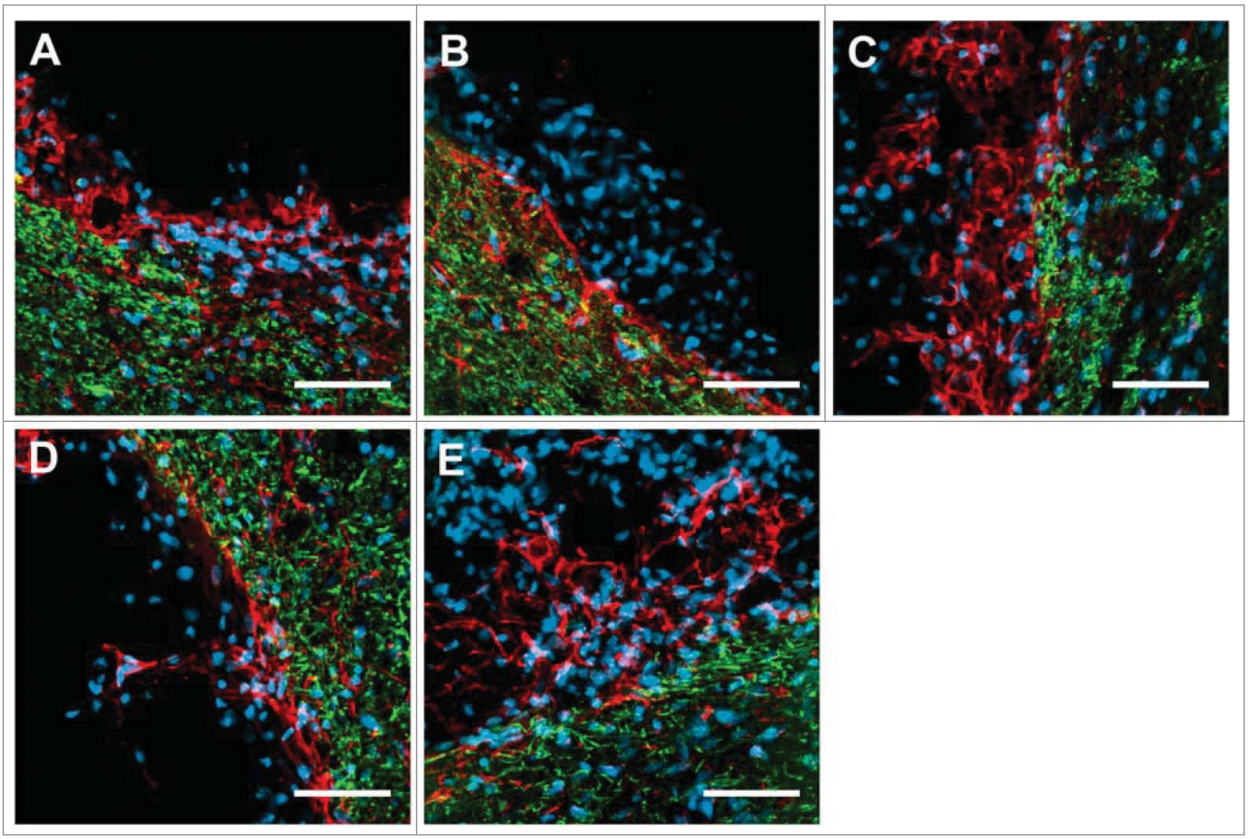

Figure 5. Images of the neurite network at the tissue-implant interface. Astrocytes (GFAP, Red), neurofilament (RT97, green), and nuclei (DAPI, blue) were stained to determine if neurite extension into the hybrid scaffold occurred. The samples were as follows: (**A**) Blank hydrogel, (**B**) PLLA fibers – low density, (**C**) PLLA + fibronectin fibers – low density, (**D**) PLLA fibers – high density, and (**E**) PLLA + fibronectin – high density. The fibronectin fiber samples, C and E, display a greater extent of astrocyte infiltration into hybrid matrix as well as a more loosely defined glial boundary as compared to that displayed in B; however, in all cases there were no neurites protruding and into the hybrid scaffold and interacting with the electrospun fiber network. Images were captured with a 40X objective lens. Z-stack ranges were optimized for each fluorescence channel and captured independently. Scale bar represents 50 μm.

fibers - low density in hydrogel, and (5) PLLA + fibronectin fibers - high density in hydrogel. An injection of saline solution served as a control (sham). Implants were analyzed at 3 time points: 7, 21, and 60 d post implantation (n = 4 for each scaffold/time point combination).

Surgical procedures were performed similar to Nisbet et al.[12] with the following alterations.

All animals were anesthetized by 2% isoflurane in oxygen, which was reduced to 0.5% upon obtaining surgical levels of anesthesia. The scaffolds, contained within 21-gauge needles, were implanted to a depth of 6 mm below the cortex surface and held in place for 5 minutes to facilitate gelation. Each implant was approximately 1.25 μL in volume. Animals were euthanized by an intraperitoneal injection of Lethabarb (100 mg/kg). A transcardial perfusion was then performed with PBS and subsequently 4% paraformaldehyde (PFA) in phosphate buffer. The brain was then removed and post fixed in 4% PFA overnight and then transferred to a 30% sucrose solution. The solution was changed daily until the tissue sank (3 days). The tissue was then snap frozen with liquid nitrogen and stored at −80°C until immunohistochemistry was performed.

Immunohistochemistry

Horizontal sections (perpendicular to the injection tract) were cut at 30 μm thickness using a cryostat. Slides were air dried for 30 minutes, post-fixed in 4% PFA for one minute, washed with phosphate buffered saline (PBS), and then blocked for 15 minutes at room temperature in a solution of 2% normal goat serum (NGS) and 0.1% Triton X100 in PBS. Each slide was then washed with PBS and immersed in antibody diluent (0.2% NGS and 0.01% Triton X100) with rabbit anti-rat glial fibrillary acid protein (Astrocytes; GFAP, Dako, Z0334), mouse anti-rat ED1 (Macrophage/Microglia; AbDSerotec, MCA314R), or anti-neurofilament (Neurons; Developmental Studies Hybridoma Bank, RT97) all diluted at 1:500 and incubated overnight at room temperature. The primary solution was removed, slides were washed, and then incubated in AlexaFluor 488 rabbit anti-mouse secondary in antibody diluent at 1:1000, and goat anti-rabbit AlexaFluor 594 for 3 hours at room temperature. Slides were then washed, incubated with DAPI at 1 ug/mL for 5 minutes, washed again, and coverslipped with anti-fade. All images were captured on an Olympus IX-81 with DSU.

Image Quantification

Images were captured using a 20X objective lens at 3 points along the implant/tissue interface of sections labeled with an anti-GFAP antibody as detailed above. The GFAP signal was quantified by first applying a standard threshold level to all images, and converting them to binary format to isolate the labeled cells from the background signal. A line was then drawn perpendicular to the implant interface, transecting the boundary. Using the plot profile function within ImageJ, the cellular signal distribution was quantified as percent area covered in increments of 25 um from the implant interface.

Disclosure of Potential Conflicts of Interest

No potential conflicts of interest were disclosed.

Funding

CJR was supported by an Endeavor Research Fellowship from the Australian Government. The project was funded, in part, by the Australian Research Council (DP0985433).

Supplemental Material

Supplemental data for this article can be accessed on the publisher's website.

References

1. Silver J, Miller JH. Regeneration beyond the glial scar. Nat Rev Neurosci 2004; 5:146-56; PMID:14735117; http://dx.doi.org/10.1038/nrn1326
2. Fawcett JW, Asher RA. The glial scar and central nervous system repair. Brain Res Bull 1999; 49:377-391; PMID:10483914; http://dx.doi.org/10.1016/S0361-9230(99)00072-6
3. Hawthorne AL, Hu H, Kundu B, Steinmetz MP, Wylie CJ, Deneris ES, Silver J. The unusual response of serotonergic neurons after CNS injury: Lack of axonal dieback and enahnced sprouting within the inhibitory environment of the glial scar. J Neurosci 2011; 31:5605-5616; PMID:21490201; http://dx.doi.org/10.1523/JNEUROSCI.6663-10.2011
4. Emerich DF, Orive G, Borlongan C. Tales of biomaterials, molecules, and cells for repairing and treating brain dysfunction. Curr Stem Cell Res Ther 2011; 6:171-89; PMID:21476979; http://dx.doi.org/10.2174/157488811796575350
5. Orive G, Anitua E, Pedraz JL, Emerich DF. Biomaterials for promoting brain protection, repair and regeneration. Nat Rev Neurosci 2009; 10:682-92; PMID:19654582; http://dx.doi.org/10.1038/nrn2685
6. Gilbert RJ, Rivet CJ, Zuidema JM, Popovich PG. Biomaterial design considerations for repairing the injured spinal cord. Crit Rev Biomed Eng 2011; 39:125-80; PMID:21488818; http://dx.doi.org/10.1615/CritRevBiomedEng.v39.i2.30
7. Nomura H, Tator CH, Shoichet MS. Bioengineered strategies for spinal cord repair. J Neurotraum 2006; 23:496-507; PMID:16629632; http://dx.doi.org/10.1089/neu.2006.23.496
8. Rahjouei A, Kiani S, Zahabi A, Mehrjardi NZ, Hashemi M, Baharvand H. Interactions of human embryonic stem cell-derived neural progenitors with an electrospun nanofibrillar surface in vitro. Int J Artif Organs 2011; 34:559-70; PMID:21786255; http://dx.doi.org/10.5301/IJAO.2011.8511
9. Xie J, Willerth SM, Li X, Macewan MR, Rader A, Sakiyama-Elbert SE, Xia Y. The differentiation of embryonic stem cells seeded on electrospun nanofibers into neural lineages. Biomaterials 2009; 30:354-62; PMID:18930315; http://dx.doi.org/10.1016/j.biomaterials.2008.09.046
10. Wang HB, Mullins ME, Cregg JM, Hurtado A, Oudega M, Trombley MT, Gilbert RJ. Creation of highly aligned electrospun poly-L-lactic acid fibers for nerve regeneration applications. J Neural Eng 2009; 6:016001; PMID:19104139; http://dx.doi.org/10.1088/1741-2560/6/1/016001
11. Hurtado A, Cregg JM, Wang HB, Wendell DF, Oudega M, Gilbert RJ, McDonald JW. Robust CNS regeneration after complete spinal cord transection using aligned poly-L-lactic acid microfibers. Biomaterials 2011; 32:6068-79; PMID:21636129
12. Nisbet DR, Rodda AE, Horne MK, Forsythe JS, Finkelstein DI. Neurite infiltration and cellular response to electrospun polycaprolactone scaffolds implanted into the brain. Biomaterials 2009; 30:4573-80; PMID:19500836; http://dx.doi.org/10.1016/j.biomaterials.2009.05.011
13. Sill TJ, von Recum HA. Electrospinning: applications in drug delivery and tissue engineering. Biomaterials 2008; 29:1989-2006; PMID:18281090; http://dx.doi.org/10.1016/j.biomaterials.2008.01.011
14. Wang TY, Forsythe JS, Nisbet DR, Parish CL. Promoting engraftment of transplanted neural stem cells/progenitors using biofunctionalised electrospun scaffolds. Biomaterials 2012; 33:9188-97; PMID:23022345; http://dx.doi.org/10.1016/j.biomaterials.2012.09.013
15. Nisbet DR, Crompton KE, Horne MK, Finkelstein DI, Forsythe JS. Neural tissue engineering of the CNS using hydrogels. J Biomed Mater Res B 2008; 87:251-63; PMID:18161806; http://dx.doi.org/10.1002/jbm.b.31000
16. Pakulska MM, Ballios BG, Shoichet MS. Injectable hydrogels for central nervous system therapy. Biomed Mater 2012; 7:024101; PMID:22456684; http://dx.doi.org/10.1088/1748-6041/7/2/024101
17. Han N, Johnson JK, Bradley PA, Parikh KS, Lanutti J, Winter JO. Cell attachment to hydrogel-electrospun fiber mat composite materials. J Funct Biomater 2012; 3:487-513; PMID:24955629; http://dx.doi.org/10.3390/jfb3030497
18. Baker BM, Gee AO, Metter RB, Nathan AS, Marklein RA, Burdick JA, Mauck RL. The potential to improve cell infiltration in composite fiber-aligned electrospun scaffolds by the selective removal of sacrificial fibers. Biomaterials 2008; 29:2348-58; PMID:18313138; http://dx.doi.org/10.1016/j.biomaterials.2008.01.032
19. Leong MF, Rasheed MZ, Lim TC, Chian KS. In vitro cell infiltration and in vivo cell infiltration and vascularization in a fibrous, highly porous poly(D,L-lactide) scaffold fabricated by cryogenic electrospinning technique. J Biomed Mater Res A 2009; 91:231-40; PMID:18814222; http://dx.doi.org/10.1002/jbm.a.32208
20. Nam J, Huang Y, Agarwal S, Lannutti J. Improved cellular infiltration in electrospun fiber via engineered porosity. Tissue Eng 2007; 13:2249-57; PMID:17536926; http://dx.doi.org/10.1089/ten.2006.0306
21. Sun B, Long YZ, Zhang HD, Li MM, Duvail JL, Jiang XY, Yin HL. Advances in three-dimensional nanofibrous macrostructures via electrospinning. Prog Polym Sci 2014; 39:862-890; http://dx.doi.org/10.1016/j.progpolymsci.2013.06.002
22. Sun B, Long YZ, Zhang HD, Li MM, Duvail JL, Jiang XY, Yin HL. Advances in three-dimensional nanofibrous macrostructures via electrospinning. Prog Polym Sci 2014; 39:862-890; http://dx.doi.org/10.1016/j.progpolymsci.2013.06.002
23. Coburn J, Gibson M, Bandalini PA, Laird C, Mao HQ, Moroni L, Seliktar D, Elisseeff J. Biomimetics of the Extracellular Matrix: An Integrated Three-Dimensional Fiber-Hydrogel Composite for Cartilage Tissue Engineering. Smart Struct Syst 2011; 7:213-22; PMID:22287978; http://dx.doi.org/10.12989/sss.2011.7.3.213
24. Hong Y, Huber A, Takanari K, Amoroso NJ, Hashizume R, Badylak SF, Wagner WR. Mechanical properties and in vivo behavior of a biodegradable synthetic polymer microfiber-extracellular matrix hydrogel biohybrid scaffold. Biomaterials 2011; 32:3387-94; PMID:21303718; http://dx.doi.org/10.1016/j.biomaterials.2011.01.025
25. Hsieh A, Zahir T, Lapitsky Y, Amsden B, Wan WK, Shoichet MS. Hydrogel/electrospun fiber composites influence neural stem/progenitor cell fate. Soft Matter 2010; 6:2227-37; http://dx.doi.org/10.1039/b924349f
26. Bosworth LA, Turner L-A, Cartmell SH. State of the art composites compromising electrospun fibers coupled with hydrogels: a review. Nanomed Nanotech Biol Med 2013; 9:322-335; http://dx.doi.org/10.1016/j.nano.2012.10.008
27. Zuidema JM, Hyzinski-Garcia MC, Van Vlasselaer K, Zaccor NW, Plopper GE, Mongin AA, Gilbert RJ. Enhanced GLT-1 mediated glutamate uptake and migration of primary astrocytes directed by fibronectin-coated electrospun poly-l-lactic acid fibers. Biomaterials 2014; 35:1439-49; PMID:24246642; http://dx.doi.org/10.1016/j.biomaterials.2013.10.079
28. Martin BC, Minner EJ, Wiseman SL, Klank RL, Gilbert RJ. Agarose and methylcellulose hydrogel blends for nerve regeneration applications. J Neural Eng 2008; 5:221-31; PMID:18503105; http://dx.doi.org/10.1088/1741-2560/5/2/013
29. Stokols S, Sakamoto J, Breckon C, Holt T, Weiss J, Tuszynski MH. Templated agarose scaffolds support linear axonal regeneration. Tissue Eng 2006; 12:2777-2787; PMID:17518647; http://dx.doi.org/10.1089/ten.2006.12.2777
30. Villapol S, Byrnes KR, Symes AJ. Temporal dynamics of cerebral blood flow, cortical damage, apoptosis, astrocyte-vasculature interaction and astrogliosis in the pericontusional region after traumatic brain injury. Front Neurol 2014; 5:1-9; PMID:24454306; http://dx.doi.org/10.3389/fneur.2014.00082
31. Koh HS, Yong T, Chan CK, Ramakrishna S. Enhancement of neurite outgrowth using nano-structured scaffolds coupled with laminin. Biomaterials 2008; 29:3574-82; PMID:18533251; http://dx.doi.org/10.1016/j.biomaterials.2008.05.014